

Topology Controlled Supramolecular Self-Assembly of Octa Triphenylene-Substituted Polyhedral Oligomeric Silsesquioxane Hybrid Supermolecules

Jianjun Miao[†] and Lei Zhu^{*,†,‡}

Polymer Program, Institute of Materials Science and Department of Chemical, Materials and Biomolecular Engineering, University of Connecticut, Storrs, Connecticut 06269-3136, and Department of Macromolecular Science and Engineering, Case Western Reserve University, Cleveland, Ohio 44106-7202

Received: October 21, 2009; Revised Manuscript Received: December 21, 2009

A series of liquid crystalline star supermolecules with polyhedral oligomeric silsesquioxane (POSS) as the central scaffold and eight triphenylenes (Tp) as the peripheral arms were synthesized via amidization reactions. The supermolecules were denoted as POSS(Tp)₈. Six POSS(Tp)₈ samples were prepared with two alkyl chain lengths in the Tp (C₅ and C₁₂) and three spacer lengths (C₂, C₆, and C₁₀) between the POSS core and the Tp arms. Three samples with C₅-Tp were amorphous because of too short alkyl chains in the Tp, while the other three samples with C₁₂-Tp self-assembled into hierarchical liquid crystalline mesophases, as studied by X-ray diffraction (XRD) and transmission electron microscopy (TEM). When the spacer length was C₂, a *column-within-column* super hexagonal columnar phase was observed, because the POSS core and the Tp arms were intimately coupled together. With increasing the spacer length to C₆ and C₁₀, respectively, the POSS core and Tp arms became gradually decoupled. Alternating POSS-Tp lamellar morphology with a rectangular columnar symmetry (by XRD) was observed by TEM for the POSS(Tp)₈ sample with a C₆-spacer. For the POSS(Tp)₈ sample with a C₁₀-spacer, an oblique columnar phase was determined by XRD, and inverted columnar morphology with four Tp columns forming a super column within the POSS/alkyl chain matrix was observed by TEM. This study suggested that molecular topology played an important role in the supramolecular self-assembly of star-shaped POSS(Tp)₈ supermolecules.

Introduction

Supermolecules are comprised of well-defined, covalently linked small molecular moieties with multifunctions and, thus, represent a novel class of advanced functional materials, which can further self-assemble into hierarchical structures.¹ Among them, supramolecular liquid crystals (LCs) are particularly interesting, because their assembly can enhance the functionality of individual liquid crystalline (LC) molecules,^{1,2} and the resulted unique physical properties are attractive for applications in advanced optoelectronic materials and biology.^{2–8} LC dendrimers belong to an interesting and important type of supramolecular LCs, where mesoscale self-assembly can be tuned by subtle modifications of the dendritic connectivity.⁹ Meanwhile, new types of mesophases and morphologies, which cannot be found in the peripheral mesogens, may be discovered.¹⁰ The self-assembly behavior of these LC dendrimers is a direct result of the interplay of (i) microphase segregation between the core and the dendrons at periphery and (ii) competition between the strong cooperative interaction among peripheral mesogens and the decreased entropy due to the deformation of the flexible core.^{9–11} The controlling structural parameters include the density and orientation of mesogenic units at periphery and the degree to which they are decoupled from the central core.¹

The first and conventional LC dendrimers were developed by Percec et al. using AB₂ type LC monomers for hyperbranching.^{12–14} Strong interactions among LC mesogens resulted in a parallel alignment of the calamitic mesogens to afford both

nematic and smectic phases, and the dendrimer cores had to deform from its original spherical shape. In novel LC dendrimers developed later, a central scaffold, either flexible or rigid, was employed as the core. For flexible scaffolds, polypropyleneimine (PPI), polyamidoamine (PAMAM), carbosiloxane, and esters have been used as the LC dendrimer core.^{15–27} In these examples, due to the rod-like mesogenic shape and the flexibility of the cores, calamitic mesophases were often observed at low generations of the dendritic cores. However, as the number density of the rod-like mesogens at periphery increased for high generation dendritic cores, columnar mesophases were observed. For example, hexagonal columnar phases were observed in PPI-based dendrimers acylated with 3,4-bis(alkyloxy)benzoic acids by Cameron et al.²⁷ McKenna et al. reported the first discotic LC dendrimers based on a PPI core.¹¹ A structural transition from rectangular columnar for the first generation to hexagonal columnar for the second to fifth generations was observed, where the discotic triphenylene (Tp) mesogens and the dendrimer core were phase separated into individual columns. In the above-mentioned calamitic to columnar mesophase transformation, the core flexibility played an important role, because a wide variety of conformers of the core were allowed for different overall shapes. So far, no thermotropic cubic mesophases have been reported in novel LC dendrimers with flexible central scaffolds, primarily due to the core flexibility and the anisotropic shape in the mesogens at periphery.

Besides flexible cores, rigid organic and inorganic molecules have also been used as the central scaffolds in LC dendrimers. Rigid organic central scaffolds include a simple benzene ring,^{28–31} an *n*-type anthraquinone,^{32,33} a *p*-type triphenylene,^{34–37} and a polyaromatic hexa-*peri*-hexabenzocoronene (HBC),³⁸ to which a defined number (mostly 6) of triphenylene,^{28,30–35}

* Corresponding author. Tel.: 216-368-5861. E-mail: lxz121@case.edu.

[†] University of Connecticut.

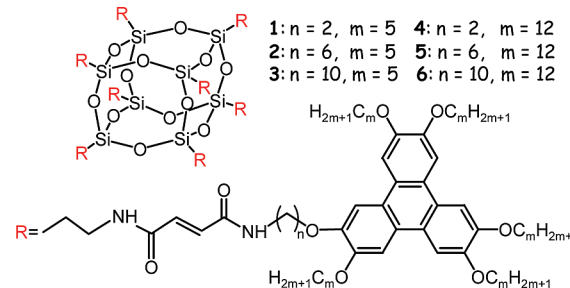
[‡] Case Western Reserve University.

HBC,³⁸ or cyanobiphenyl^{36,37} mesogens were attached via ester, siloxane, or ether bonds. For Tp-armed LC star molecules, a normal hexagonal columnar phase with the unit cell dimension equivalent to that for the parent Tp discotic LCs was often observed, regardless of the type of the central cores.^{28,30–35,38} Due to the covalent bonding of the peripheral Tp mesogens to the central core, a disordered superlattice based on the central cores was sometimes seen.^{30,31,35} A broad temperature range for the LC phase was obtained as compared with the parent Tp LCs.^{30,31,35} For cyanobiphenyl-armed Tp star molecules, a biaxial nematic phase was observed with short spacers³⁷ and a rich polymorphism existed with a long spacer between the Tp core and the cyanobiphenyl arms.³⁶

Examples of rigid inorganic central scaffolds include cyclo-triphosphazene, fullerene (C_{60}), and polyhedral oligomeric silsesquioxane (POSS). Although most calamitic mesogen-substituted cyclotriphosphazene exhibited calamitic (nematic or smectic) phases,^{39–41} a hexagonal columnar phase was found at high temperatures for polycatenar substituted or complexed cyclotriphosphazenes.^{42,43} For C_{60} -based thermotropic LC dendrimers, different numbers of calamitic mesogens were covalently linked to the C_{60} core via either mono- or hexa-adduction.^{44–48} Calamitic mesophases (e.g., smectic A) were often observed with the formation of microphase segregated C_{60} layers. When one or two poly(benzyl ether) dendrons were grafted onto the C_{60} core as a monoadduct, columnar mesophases (rectangular for the second generation^{49,50} and hexagonal for the third generation⁵⁰) were observed. In these columnar phases, two C_{60} monoadducts with two second- and third-generation dendrons or several C_{60} monoadducts with one second-generation dendron aggregated together to form a full disk.

Cubic-shaped POSS is a unique nanobuilding block with multifunctionalities and, thus, has been employed as a rigid central scaffold for novel LC dendrimers. For an octa substituted POSS with 8 or 16 end-attached calamitic mesogens, smectic (A and/or C) phases with alternating POSS and mesogen layers were often observed.^{51–54} To induce nematic (including chiral nematic) phases, two methods were employed. The first method involved lateral attachment of (chiral) calamitic mesogens to the POSS core,^{55–58} and the second method used partial (four) substitution of the POSS core.^{59,60} Intriguingly, rectangular and hexagonal columnar mesophases were observed at temperatures below the nematic phase for POSS-based LCs with laterally attached mesogens.^{57,58,61,62} In these columnar assemblies, central POSS cores formed the column, and peripheral rod-like mesogens oriented with their molecular long axes roughly parallel to the column axis. In a novel type of POSS LC supermolecules, eight bend-core mesogens were end-attached to the POSS core via hydrosilylation.⁶³ Without an electric field, the bend-core mesogens formed an antiferroelectric smectic C layer alternating with a POSS layer. Although the POSS-calamitic LC supermolecules have been extensively studied, there are only a few studies focusing on POSS LC supermolecules with discotic mesogens at periphery. Recently, a POSS-triphenylene dyad molecule was reported, a lamello-columnar phase was observed.⁶⁴ Due to the asymmetry in a POSS-Tp dyad molecule, POSS crystallized into an ABCA (i.e., a trigonal symmetry) four-layer crystalline lamella, and Tps formed a homeotropic nematic discotic LC sandwiched between neighboring POSS crystalline lamellae.

In this report, we successfully attached eight Tp monoamines to a POSS octa amino acid molecule via the amidization reaction. The supermolecules were denoted as POSS(Tp)₈. By



varying the alkyl chain length (C_5 and C_{12}) in Tp and the spacer length (C_2 , C_6 , and C_{10}) between the POSS core and the Tp arms, different mesophase self-assemblies in these cube-disk supermolecules were observed by X-ray diffraction (XRD) and transmission electron microscopy (TEM) techniques. When the spacer length (C_2) was much shorter than the alkyl chain length (C_{12}) in the Tp arms, the POSS core and the Tp arms joined together to form a superdisk, which further stacked together to form a “column-within-column” hexagonal columnar phase. With increasing the spacer length to C_6 and C_{10} , the POSS core and the Tp arms became decoupled, and thus, rectangular or hexagonal columnar phases were observed.

Experimental Section

Materials. POSS octa amic acid was purchased from Hybrid Plastics, Inc. (Hattiesburg, MS). Benzotriazol-1-yl-oxytritypyrrolidinophosphonium hexafluorophosphate (PyBOP) and *N,N*-diisopropylethylamine were purchased from Aldrich. Triphenylene monoamines were synthesized according to literature with certain modifications.^{30,31} All solvents were purchased from Fisher Scientific and used without further purification.

General Synthesis Procedure and Characterization for Samples 1–6. A total of 20 mg (0.012 mmol) of POSS octamic acid was activated by 58 mg (0.11 mmol) of PyBOP and 1 drop of *N,N*-diisopropylethylamine in 5 mL of anhydrous *N,N*-dimethylformamide (DMF). The mixture solution was sonicated for 10 min at room temperature, followed by addition of 0.22 mmol of the corresponding Tp monoamine (160 mg for **1**, 172 mg for **2**, 184 mg for **3**, 266 mg for **4**, 280 mg for **5**, and 294 mg for **6**; see chemical structures in Scheme 1). The reaction mixture was further sonicated at room temperature for 30 min, and the completion of reaction was checked by thin layer chromatography (TLC) using 10 vol % methanol in chloroform as the developing solvent. The reaction mixture was then poured into 20 mL of double-distilled water and extracted with 10 mL of chloroform three times. The combined organic fractions were washed with 20 mL of 1 N HCl, 20 mL of 0.9 M NaHCO₃, and 20 mL of brine, respectively, before drying over anhydrous MgSO₄. After filtration and removal of the solvent under vacuum, crude products were purified by column chromatography (silica gel, chloroform/methanol 90:5). Pure yellow to brown solids were obtained with yields: 59% for **1**, 49% for **2**, 51% for **3**, 60% for **4**, 55% for **5**, and 52% for **6**. Samples **1–3** are abbreviated as POSS(5Tp)₈ and samples **4–6** are abbreviated as POSS(12Tp)₈, where 5 and 12 denote that the alkyl chains in Tp are C₅ and C₁₂, respectively.

The purity of all samples was checked by TLC, proton and carbon nuclear magnetic resonance spectroscopy (^1H and ^{13}C NMR), and size-exclusion chromatography (SEC). As shown in Figure 1, sharp unimodel peaks for all samples were obtained, and the polydispersity indices (PDIs) were between 1.02 and

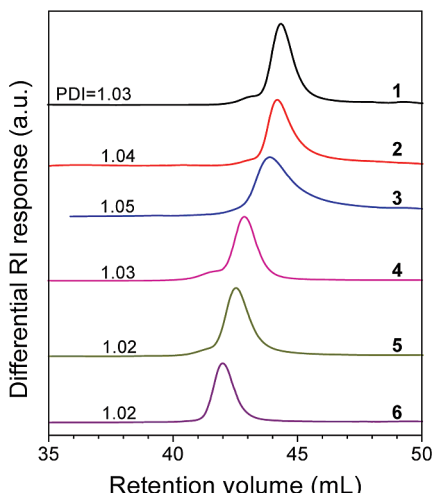


Figure 1. Size-exclusion chromatography (SEC) curves for POSS(Tp)₈ supermolecules **1–6**.

1.05. The gradual increase in the peak tail at high retention volumes from **1** to **3** could be attributed to an increased tendency of the bisamide group adsorption onto SEC columns because of an increased flexibility in the spacers between the POSS core and the Tp arms, as well as less steric protection from C₅-alkyl chains as compared to C₁₂-alkyl chains in samples **4–6**.

¹H NMR for **1** (CDCl₃): 0.68 (16H, m, Si-CH₂), 1.0–0.85 (120H, m, CH₃), 2.0–1.2 (240H, m, CH₂ in alkyl tails), 3.29 (32H, m, CH₂NHCO), 4.3–4.15 (96H, m, OCH₂), 6.15–6.0 (8H, m, NHCO), 7.82 (48H, m, triphenylene Tp-H). ¹³C NMR for **1** (CDCl₃): 14.1 (s, CH₃), 22.7 (s, SiCH₂ and CH₃CH₂), 25.7–26.3 (s, OCH₂CH₂CH₂), 26.9 (s, SiCH₂CH₂), 29.4–29.7 (s, OCH₂CH₂), 31.9 (s, CH₃CH₂CH₂), 39.0 (s, CONHCH₂), 69.7 (s, OCH₂), 107.4 (s, 6C, aromatic), 123.7 (s, 6C, aromatic), 132.6 (NHCOCHCHCONH), 149.0 (s, 6C, aromatic), 164.9 (s, NHCO).

¹H NMR for **2** (CDCl₃): 0.68 (16H, m, Si-CH₂), 1.0–0.85 (120H, m, CH₃), 2.0–1.2 (304H, m, CH₂ in alkyl tails), 3.29 (32H, m, CH₂NHCO), 4.3–4.15 (96H, m, OCH₂), 6.15–6.0 (8H, m, NHCO), 7.82 (48H, m, triphenylene Tp-H). ¹³C NMR for **2** (CDCl₃): 14.1 (s, CH₃), 22.7 (s, SiCH₂ and CH₃CH₂), 25.7–26.3 (s, OCH₂CH₂CH₂), 26.9 (s, SiCH₂CH₂ and NHCH₂CH₂CH₂), 29.4–29.7 (s, OCH₂CH₂, NHCH₂CH₂ and NHCH₂CH₂CH₂(CH₂)₂), 31.9 (s, CH₃CH₂CH₂), 40.2 (s, NHCH₂), 69.7 (s, OCH₂), 107.4 (s, 6C, aromatic), 123.7 (s, 6C, aromatic), 132.6 (NHCOCHCHCONH), 149.0 (s, 6C, aromatic), 164.9 (s, NHCO).

¹H NMR for **3** (CDCl₃): 0.68 (16H, m, Si-CH₂), 1.0–0.85 (120H, m, CH₃), 2.0–1.2 (368H, m, CH₂ in alkyl tails), 3.25 (32H, m, CH₂NHCO), 4.3–4.15 (96H, m, OCH₂), 6.15–6.0 (8H, m, NHCO), 7.82 (48H, m, triphenylene Tp-H). ¹³C NMR for **3** (CDCl₃): 14.1 (s, CH₃), 22.7 (s, SiCH₂ and CH₃CH₂), 25.7–26.3 (s, OCH₂CH₂CH₂), 26.9 (s, SiCH₂CH₂ and NHCH₂CH₂CH₂), 29.4–29.7 (s, OCH₂CH₂, NHCH₂CH₂ and NHCH₂CH₂CH₂(CH₂)₆), 31.9 (s, CH₃CH₂CH₂), 40.2 (s, NHCH₂), 69.7 (s, OCH₂), 107.4 (s, 6C, aromatic), 123.7 (s, 6C, aromatic), 132.6 (NHCOCHCHCONH), 149.0 (s, 6C, aromatic), 164.9 (s, NHCO).

¹H NMR for **4** (CDCl₃): 0.68 (16H, m, Si-CH₂), 1.0–0.85 (120H, m, CH₃), 2.0–1.2 (800H, m, CH₂ in alkyl tails), 3.3 (32H, m, CH₂NHCO), 4.3–4.15 (96H, m, OCH₂), 6.15–6.0 (8H, m, NHCO), 7.82 (48H, m, triphenylene Tp-H). ¹³C NMR for **4** (CDCl₃): 14.1 (s, CH₃), 22.7 (s, SiCH₂ and CH₃CH₂), 25.7–26.3 (s, OCH₂CH₂CH₂), 26.9 (s, SiCH₂CH₂), 29.4–29.7

(s, OCH₂(CH₂)₇CH₂CH₂CH₃ and NHCH₂CH₂), 31.9 (s, CH₃CH₂CH₂), 39.0 (s, CONHCH₂), 69.7 (s, OCH₂), 107.4 (s, 6C, aromatic), 123.7 (s, 6C, aromatic), 132.6 (NHCOCHCHCONH), 149.0 (s, 6C, aromatic), 164.9 (s, NHCO).

¹H NMR for **5** (CDCl₃): 0.68 (16H, m, Si-CH₂), 1.0–0.85 (120H, m, CH₃), 2.0–1.2 (864H, m, CH₂ in alkyl tails), 3.3 (32H, m, CH₂NHCO), 4.3–4.15 (96H, m, OCH₂), 6.15–6.0 (8H, m, NHCO), 7.82 (48H, m, triphenylene Tp-H). ¹³C NMR for **5** (CDCl₃): 14.1 (s, CH₃), 22.7 (s, SiCH₂ and CH₃CH₂), 25.7–26.3 (s, OCH₂CH₂CH₂), 26.9 (s, SiCH₂CH₂ and NHCH₂CH₂CH₂), 29.4–29.7 (s, OCH₂(CH₂)₇CH₂CH₂CH₃ and NHCH₂CH₂CH₂), 31.9 (s, CH₃CH₂CH₂CH₃), 40.2 (s, NHCH₂CH₂CH₂CH₃), 69.7 (s, OCH₂), 107.4 (s, 6C, aromatic), 123.7 (s, 6C, aromatic), 132.6 (NHCOCHCHCONH), 149.0 (s, 6C, aromatic), 164.9 (s, NHCO).

¹H NMR for **6** (CDCl₃): 0.68 (16H, m, Si-CH₂), 1.0–0.85 (120H, m, CH₃), 2.0–1.2 (928H, m, CH₂ in alkyl tails), 3.29 (32H, m, CH₂NHCO), 4.3–4.15 (96H, m, OCH₂), 6.15–6.0 (8H, m, NHCO), 7.82 (48H, m, triphenylene Tp-H). ¹³C NMR for **6** (CDCl₃): 14.1 (s, CH₃), 22.7 (s, SiCH₂ and CH₃CH₂), 25.7–26.3 (s, OCH₂CH₂CH₂), 26.9 (s, SiCH₂CH₂ and NHCH₂CH₂CH₂), 29.4–29.7 (s, OCH₂(CH₂)₇CH₂CH₂CH₃, NHCH₂CH₂CH₂ and NHCH₂CH₂CH₂(CH₂)₆), 31.9 (s, CH₃CH₂CH₂CH₃), 40.2 (s, NHCH₂CH₂CH₂CH₃), 69.7 (s, OCH₂), 107.4 (s, 6C, aromatic), 123.7 (s, 6C, aromatic), 132.6 (NHCOCHCHCONH), 149.0 (s, 6C, aromatic), 164.9 (s, NHCO).

Instrumentation and Characterization. ¹H and ¹³C NMR spectra were recorded on a Bruker spectrometer (500 MHz, DMX 500). Fourier transform infrared (FTIR) was performed on a Nicolet Magna 560 FTIR spectrometer. Differential scanning calorimetry (DSC) experiments were carried out on a TA DSC-Q100 instrument. An indium standard was used for both temperature and enthalpy calibrations. An approximately 1–3 mg sample was used for the DSC study and the scanning rate was 10 °C/min. SEC was performed on a Viscotek GPCmax VE2001 with quadruple detectors (RI, UV-vis, viscometer, and light scattering). THF was used as solvent and polystyrene standards were used for calibration. Polarized light microscopy (PLM) experiments were performed using an Olympus BX51P microscope equipped with an Instec HCS410 hot stage.

2D X-ray diffraction (XRD) experiments were performed at the synchrotron X-ray beamline X27C at National Synchrotron Light Source, Brookhaven National Laboratory. The wavelength of X-ray was 0.1371 nm. The scattering angle was calibrated using silver behenate with the primary reflection peak at a scattering vector $q = (4\pi \sin \theta)/\lambda = 1.076 \text{ nm}^{-1}$, where θ is the half-scattering angle and λ is the wavelength. Fuji imaging plates were used as detectors for XRD experiments, and digital images were obtained using a Fuji BAS-2500 scanner. The typical data requisition time was 1 min. An Instec HCS410 hot stage equipped with a liquid-nitrogen cooling accessory was used in temperature-dependent X-ray experiments. One-dimensional (1D) XRD profiles were obtained by integration of the corresponding 2D XRD patterns.

TEM experiments were performed on a Philips EM300 at an accelerating voltage of 80 kV. Thin sections with thicknesses about 75–100 nm were obtained using a Leica Ultracut UCT microtome with a glass knife. Thin section samples were collected onto 400 mesh TEM grids, freeze-dried, and stained in RuO₄ vapor at room temperature for 20–30 min.⁶⁵

To measure the density of samples, 0.1–0.2 mm thick bubble-free films were obtained by annealing in a vacuum oven above its melting point. A small piece (ca. 1 mm × 1 mm) of the sample film was immersed in methanol, to which a saturated

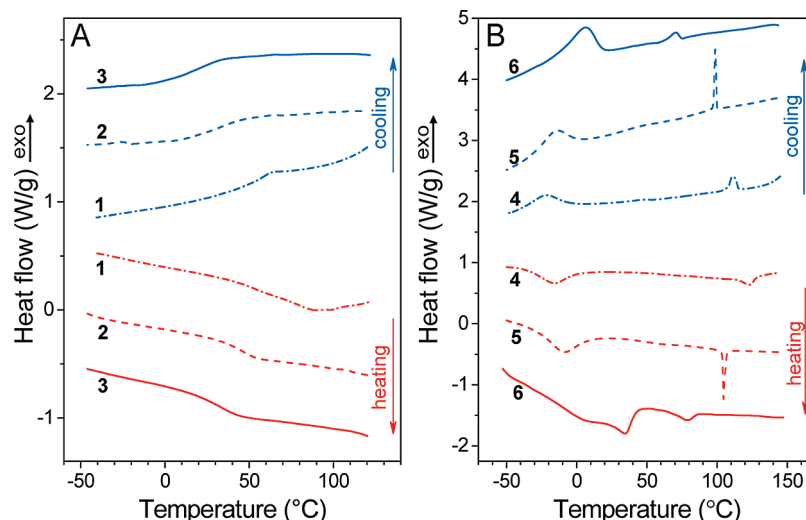


Figure 2. DSC first cooling and second heating curves for (A) POSS(5Tp)₈ **1–3** and (B) POSS(12Tp)₈ **4–6**, respectively. The scanning rate is 10 °C/min.

NaCl aqueous solution was dropwise added until the sample film suspended in the solution without settling down to the bottom or floating up to the surface for at least 5 h. The density of the solution was measured by a density bottle and thus taken as the density of the sample.

Results and Discussion

Thermal Behavior and Morphology Studied by DSC and PLM. Figure 2A shows the first cooling and second heating DSC curves for the POSS(5Tp)₈ **1–3** with short C₅ arms in the Tp. Only glass transitions were observed, and no birefringence was observed under PLM, indicating that the POSS(5Tp)₈ **1–3** were amorphous. With increasing the spacer length from C₂ for sample **1** to C₁₀ for sample **3**, the glass transition temperature (T_g) decreased from 69.0 to 31.7 °C upon heating.

Figure 2B shows the first cooling and second heating DSC curves for the POSS(12Tp)₈ **4–6** with long C₁₂ arms in the Tp. Different from the POSS(5Tp)₈, they exhibited two major phase transitions with one at high temperatures and the other at low temperatures. For example, sample **4** showed a relatively sharp peak at 111 °C (32.5 kJ/mol) and a broad peak at -22 °C (119 kJ/mol) during cooling. Two reverse processes took place with peaks at -16 °C (145 kJ/mol) and 123 °C (47.5 kJ/mol), respectively, upon heating. Judging from the magnitude of heats of transition, the high temperature transition during heating was a LC isotropization process, and the low temperature transition upon cooling should be the entire molecule crystallization induced by C₁₂-alkyl chains (similar C₁₂-induced crystallization of entire supermolecules was also observed in a previous study⁶⁶). During heating, the crystal melting temperature gradually increased from -16 °C for sample **4** to -9 °C for sample **5** and finally to 34 °C for sample **6**. The LC isotropization temperature gradually decreased from 123 °C for sample **4** to 105 °C for sample **5** and finally to 78 °C for sample **6**. Again, this can be attributed to the effect of the spacer length in POSS(Tp)₈ supermolecules. When the spacer length is very short (C₂), as compared to the alkyl arm length (C₁₂), the whole molecule becomes rigid, and both the C₁₂-alkyl chain-induced crystallization and the subsequent LC isotropization become difficult. When the spacer length increases, the flexibility in the POSS(12Tp)₈ supermolecules improves. As a result, the C₁₂-alkyl chain-induced crystallization and the subsequent LC isotropization become easier. Thermal behaviors of samples **1–6** are summarized in Table 1.

TABLE 1: Phase Transition Peak Temperatures (°C, above the arrow) and Heats of Transition (kJ/mol, below the arrow) for POSS(Tp)₈ Samples **1–6**

samples	first cooling	second heating
1	I $\xrightarrow{55.1}$ g	g $\xrightarrow{69.0}$ I
2	I $\xrightarrow{31.5}$ g	g $\xrightarrow{43.9}$ I
3	I $\xrightarrow{19.3}$ g	g $\xrightarrow{31.7}$ I
4	I $\xrightarrow{111}$ Col _{ho} $\xrightarrow{-22}$ Cr	Cr $\xrightarrow{-16}$ Col _{ho} $\xrightarrow{123}$ I
	32.5	145
	99	47.2
5	I $\xrightarrow{26.9}$ Col _{ro} ^L $\xrightarrow{-15}$ Cr	Cr $\xrightarrow{-9}$ Col _{ro} ^L $\xrightarrow{105}$ I
	71	163
	14	26.9
6	I $\xrightarrow{Col_{oo}}$ Cr	Cr $\xrightarrow{34}$ Col _{oo} $\xrightarrow{78}$ I
	232	261
	5.6	15.4

^a Cr = crystal; g = glass; Col_{ho} = ordered hexagonal columnar phase; Col_{ro}^L = ordered rectangular columnar phase with a lamellar feature; Col_{oo} = ordered oblique columnar phase; I = isotropic.

The PLM image for sample **4** in Figure 3A shows a leaf-like texture at 109 °C, which is a typical texture for hexagonal columnar phases. After cooling to room temperature, a mixture of the leaf-like texture and small crystalline grains was observed in Figure 3B. For samples **5** and **6**, focal-conic-like textures were observed (Figure 3C and D). For both samples **5** and **6**, the high temperature LC textures differed very little from those after cooling to the solid state at low temperatures.

Phase Structures Characterized by XRD and TEM Studies. Supramolecular self-assembly of the star supermolecules **4–6** were studied by XRD and TEM. Figure 4A shows 1D XRD profiles for sample **4** during cooling from the isotropic melt. At 150 °C, two amorphous halos were observed in both the low- and high-angle regions. At low angles, the peak of the halo was located at $q = 1.56 \text{ nm}^{-1}$, corresponding to a *d*-spacing of 4.03 nm. This is close to the size of the entire supermolecule (~5 nm). Therefore, it can be attributed to the average distance among randomly packed neighboring supermolecules. The high-angle amorphous halo at 13.47 nm^{-1} (0.466 nm) was attributed to the average distance among amorphous alkyl chains. At 100 °C, sharp reflection peaks were observed in the low-angle region

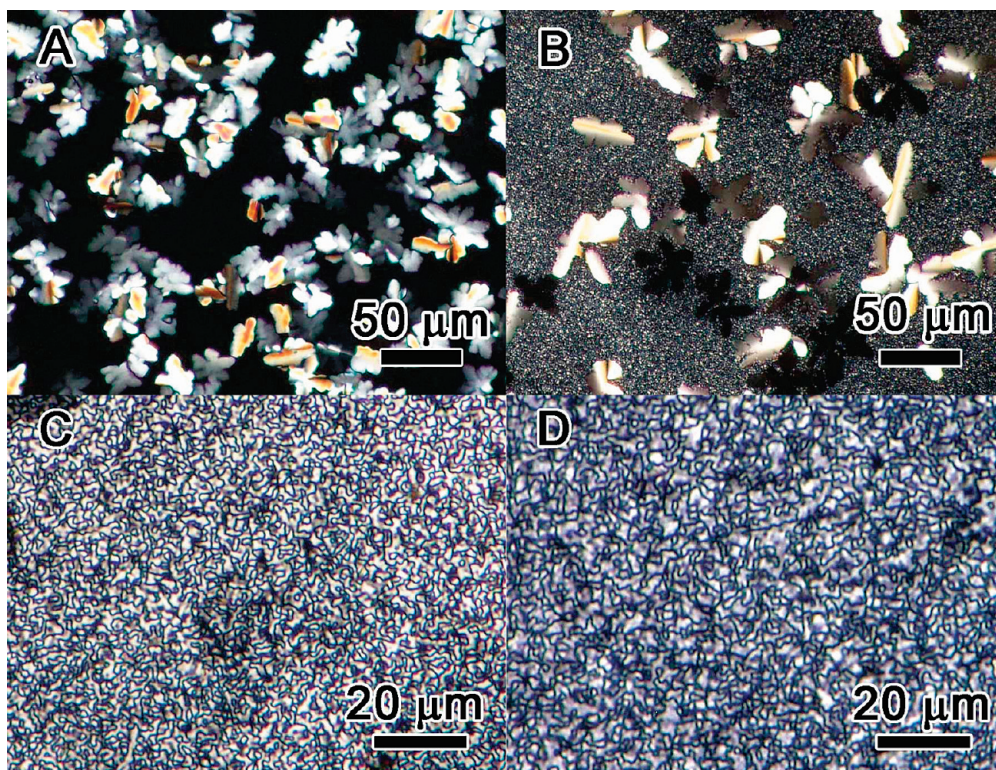


Figure 3. PLM micrographs for POSS(12Tp)₈ samples: (A) **4** at 109 °C, (B) **4** at room temperature, (C) **5**, and (D) **6** at room temperature after slow cooling from the isotropic melt.

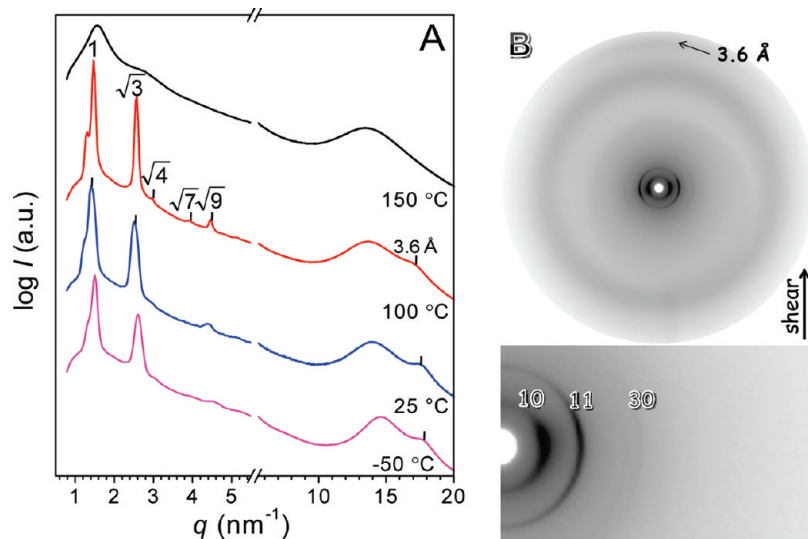


Figure 4. (A) 1D XRD profiles at different temperatures and (B) 2D XRD pattern of shear-oriented POSS(12Tp)₈ sample **4** at room temperature. Miller indices for reflections are shown in the XRD pattern in (B). Due to space limitation, all $(hk0)$ reflections are shown only as (hk) on the equator.

with a q -relationship being $1:\sqrt{3}:\sqrt{4}:\sqrt{7}:\sqrt{9}$. Thus, a hexagonal columnar structure was determined for sample **4** [see the matching of observed and calculated reflections in Table S1 in the Supporting Information (SI)]. Judging from the first-order peak at 1.476 nm^{-1} , the distance between neighboring columns was 4.92 nm. Because this distance again was similar to the whole molecule size of $\sim 5 \text{ nm}$, we consider that the entire supermolecules stack together to form an LC column. In the high-angle region, a broad reflection peak was observed at 17.2 nm^{-1} , which corresponded to a d -spacing of 0.365 nm. This is a typical $\pi-\pi$ stacking distance for ordered Tp columnar LCs.⁶⁷ With gradually decreasing the temperature to $-50 \text{ }^\circ\text{C}$, the whole supermolecules crystallized, as induced by the C₁₂-alkyl chain

crystallization. This crystallization resulted in broader reflections and disappearance of some high q reflections in the low-angle region. However, the general hexagonal columnar feature was largely preserved, suggesting that the C₁₂-alkyl chain-induced crystallization did not destroy the columnar packing. Figure 4B shows the 2D XRD pattern of the shear-oriented sample **4** (the shear temperatures were a few to 20 °C below the isotropization temperature). Clearly, the (100), (110), and (300) reflections were observed on the equator at low angles, indicating that the hexagonally packed columns were oriented along the shear direction. In the high-angle region, the Tp $\pi-\pi$ stacking reflection (0.365 nm) was observed on the meridian, suggesting that the Tp disks oriented perpendicular to the columns.

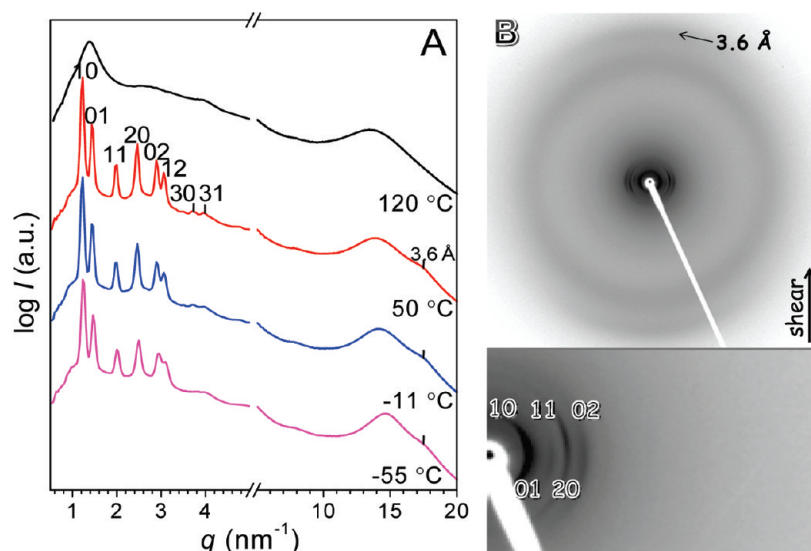


Figure 5. (A) 1D XRD profiles at different temperatures and (B) 2D XRD pattern of shear-oriented POSS(12Tp)₈ sample **5** at room temperature. Miller indices for reflections are shown in the XRD pattern in (B). Due to space limitation, all $(hk0)$ reflections are shown only as (hk) on the equator.

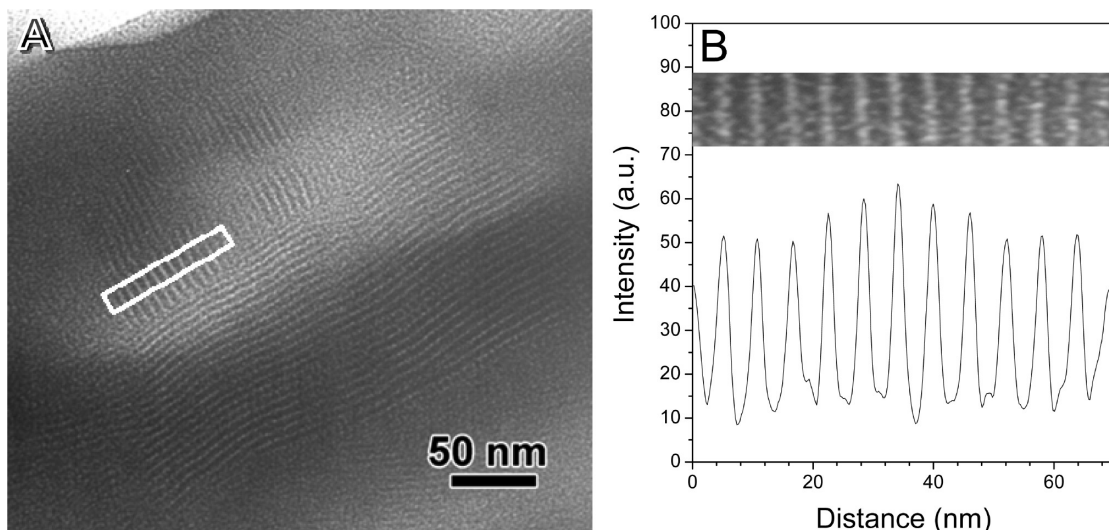


Figure 6. (A) Bright-field TEM micrograph for POSS(12Tp)₈ sample **5** showing lamellar morphology. (B) 1D intensity profile scan of the TEM image in the frame in (A). The thin section was stained by RuO₄ vapor for 30 min.

The supramolecular self-assembly of the POSS(12Tp)₈ **5** was studied by temperature-dependent 1D XRD, as shown in Figure 5A. The isotropic melt at 120 °C again showed two amorphous halos at 1.383 (4.54 nm) and 13.50 nm⁻¹ (0.465 nm), respectively. The low-angle halo represented the average distance among randomly packed supermolecules. When the temperature decreased to 50 °C, sharp reflection peaks were observed at low angles, and a weak Tp $\pi-\pi$ stacking reflection was observed at 17.4 nm⁻¹ (0.36 nm). To solve the LC structure, 2D XRD experiments were performed on the shear-oriented sample. All low angle reflections were observed on the equator, and thus, they could be fitted using a 2D rectangular structure: $a = 5.10$ nm, $b = 4.35$ nm (see the matching of observed and calculated reflections in Table S2 in the SI). The Tp $\pi-\pi$ stacking reflection was seen on the meridian, again indicating that the Tp disks were oriented perpendicular to the columns. With further decreasing the temperature to -55 °C, the whole supermolecules crystallized as induced by the C₁₂-alkyl chain crystallization. The reflections at low angles became broader; however, the rectangular columnar feature preserved.

The mesoscale morphology in sample **5** was studied by TEM on microtomed thin sections stained by RuO₄, as shown in Figure 6A. Intriguingly, well-ordered lamellar morphology, instead of individual Tp columns, was observed. Because RuO₄ did not stain POSS,⁶⁸ POSS domains appeared bright and the Tp domains appeared dark in the TEM micrograph. To obtain detailed information on molecular packing, the TEM image in the white frame in Figure 6A was analyzed and the result is shown in Figure 6B. From this analysis, the average white (POSS) domain thickness was 1.3 nm and the average dark (Tp) domain thickness was 3.8 nm. An isobutyl-substituted POSS has a diameter of ~1.0 nm⁶⁸ and a C₁₂-Tp disk has a diameter of ~2.5 nm.⁶⁹ Therefore, we conclude that the Tp lamella should consist of a double-layer of Tp columns and the POSS lamella had a single layer. The registry among neighboring lamellae was so regular that a 2D rectangular symmetry was obtained.

The supramolecular self-assembly of sample **6** was again studied by temperature-dependent 1D XRD, as shown in Figure 7A. In the isotropic melt, two amorphous halos were observed, with the low-angle halo (1.266 nm⁻¹) representing the average

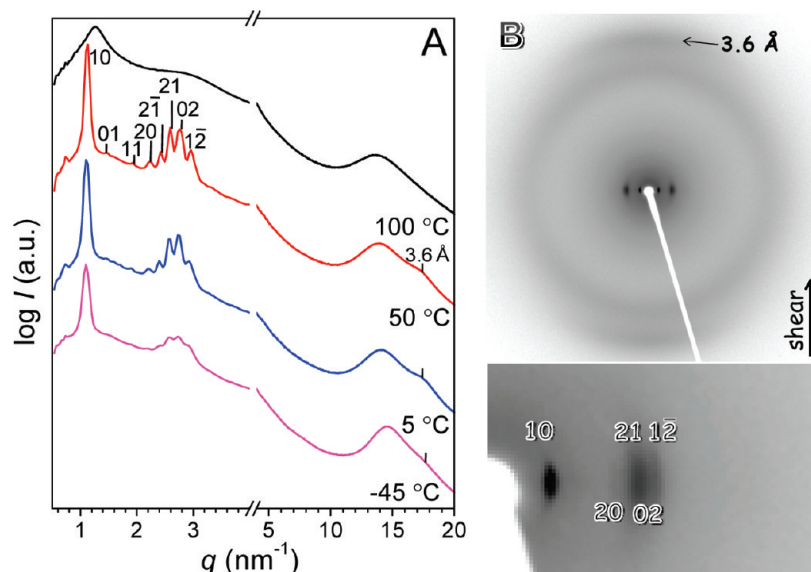


Figure 7. (A) 1D XRD profiles at different temperatures and (B) 2D XRD pattern of shear-oriented POSS(12Tp)₈ sample **6** at room temperature. Miller indices for reflections are shown in the XRD pattern in (B). Due to space limitation, all (hk0) reflections are shown only as (hk) on the equator.

distance (4.96 nm) among randomly packed supermolecules. When the temperature decreased to 50 °C, multiple sharp reflections were observed in the low-angle region, indicating a well-ordered LC structure in the sample. At high angles, a weak reflection was observed at 17.4 nm⁻¹ (0.36 nm), representing an ordered $\pi-\pi$ stacking of the Tp in a LC column. To solve the LC structure in sample **6**, 2D XRD experiments were carried out on a shear-oriented sample (see Figure 7B). The low-angle reflections were exclusively observed on the equator, and thus, a 2D oblique symmetry was determined for the structure: $a = 5.75$ nm, $b = 4.36$ nm, and $\gamma = 98^\circ$ (see the matching of observed and calculated reflections in Table S3 in the SI). The ordered Tp $\pi-\pi$ stacking reflection was again observed on the meridian, suggesting a perpendicular orientation of the disks with respect to the column axes. With further decreasing the temperature to -45 °C, the entire supermolecules crystallized as induced by the C₁₂-alkyl chain crystallization. The low-angle peaks became less intensive and broader; however, the oblique columnar feature remained intact in the sample.

The mesoscale morphology in sample **6** was studied by TEM on microtomed thin sections stained by RuO₄, as shown in Figure 8. Individual dark columns were observed when the viewing angles were perpendicular to (Figure 8A) and along the columns (Figure 8B). Considering the volume fraction of POSS in the supermolecules (~20 vol %), POSS should form the columns and Tp should be the matrix. Interestingly, the columns were formed by the Tp arms instead of the POSS cores, because the columns appeared dark (stained by RuO₄) in the TEM micrograph in Figure 8B. Calculated from the TEM images, the dark columns had a diameter of about 3.8 nm and the bright shells had a thickness of about 1.3 nm. Taking into account the C₁₂-Tp disk diameter (ca. 2.5 nm)⁶⁹ and POSS diameter (ca. 1.0 nm),⁶⁸ one dark column in Figure 8B could accommodate four Tps and the bright shell should consist of one layer of POSS.

Figure 9 summarizes the supramolecular self-assembly of POSS(12Tp)₈ supermolecules with various spacer lengths. Although there was hydrogen-binding in the POSS(12Tp)₈ supermolecules due to 16 amide groups, we found by Fourier transform infrared study that hydrogen-bonding existed both below and above the isotropization temperatures, regardless of

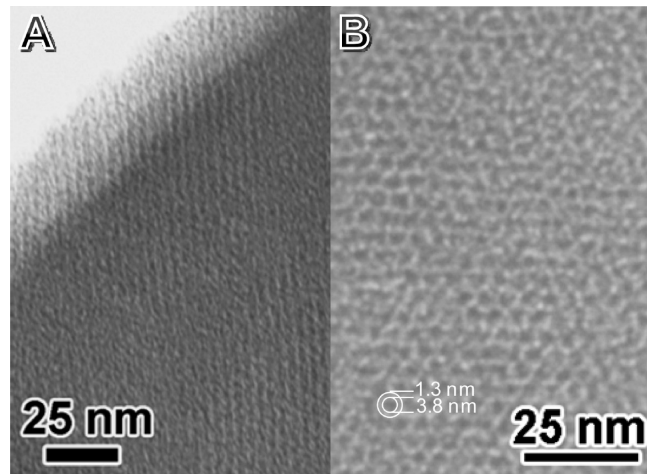


Figure 8. Bright-field TEM micrographs for the POSS(12Tp)₈ sample **6** with views (A) perpendicular to and (B) along the columns. The thin section was stained by RuO₄ vapor for 30 min.

the disordering of the supramolecular self-assemblies (see Figure S1 in the SI). Therefore, we consider that molecular shape and topology is more important for the supramolecular self-assembly of POSS(Tp)₈ supermolecules. When the spacer length, for example, C₂ in sample **4**, is much shorter than the Tp C₁₂-alkyl chains, the Tp arms are tightly attached to the POSS core, and thus, the supermolecules adopt a disk-like overall molecular shape when they stack in parallel together. Finally, a *column-within-column* nanostructure is obtained; four Tp columns inside a supercolumn formed by the entire supermolecules (see the top panel of Figure 9). Assuming one molecule per unit cell (area = 20.96 nm²) and the thickness per molecule = 0.72 nm (i.e., 2 × 0.36 nm), the density of sample **4** is estimated to be 1.218 g/cm³. When the spacer length increases to C₆ in sample **5**, Tp arms are decoupled from the POSS core to a certain extent. The supermolecules therefore adopt a board-like overall molecular shape, and a lamellar structure with a 2D rectangular symmetry is obtained. Assuming one molecule per unit cell (area = 22.18 nm²) and the thickness per molecules = 0.72 nm, the density of sample **5** is estimated to be 1.198 g/cm³. When the spacer length further increases to C₁₀ in sample **6**, Tp arms

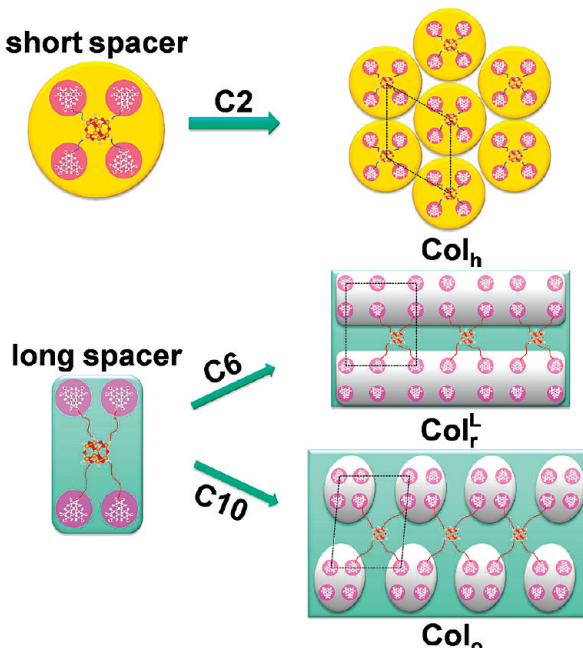


Figure 9. Schematic representations of the supramolecular self-assembly of POSS(12Tp)₈ supermolecules **4–6** with C₂, C₆, and C₁₀ spacer lengths, respectively. 2D unit cells are shown in dotted lines.

become fairly mobile and thus four Tp columns aggregate together (i.e., segregated from the POSS core) to form a supercolumn as observed in the TEM micrograph in Figure 8B. Again, because POSS cannot be stained by RuO₄, the Tp supercolumns appear dark. Assume one molecule per unit cell (area = 24.83 nm²) and the thickness per molecule = 0.72 nm, the density of sample **6** is estimated to be 1.112 g/cm³. All these estimated densities are consistent with experimental densities; 1.16 g/cm³ for sample **4**, 1.147 g/cm³ for sample **5**, and 1.055 g/cm³ for sample **6**. In these schematic drawings, terminal alkyl chains in Tp arms occupy the rest of spaces other than the Tp columns and the POSS core. Meanwhile, these alkyl chains of adjacent supermolecules can interdigitate, thus, forming a uniform alkyl chain environment.

Conclusions

A series of well-defined POSS(Tp)₈ supermolecules were synthesized with two alkyl chain lengths (C₅ and C₁₂) in the Tp arms and three spacer lengths (C₂, C₆, and C₁₀) between the POSS core and the Tp arms. When the alkyl chains in the Tp were short (i.e., C₅), no self-assembly was observed in the amorphous samples at all temperatures studied. When alkyl chains in the Tp were long (i.e., C₁₂), hierarchical LC self-assembly was observed. 2D XRD and TEM techniques were used to identify the mesophase structures of these ordered POSS(12Tp)₈ samples. When the spacer length was very short (C₂), the POSS core and the Tp arms were intimately coupled together, and thus, a *column-within-column* super hexagonal columnar phase was obtained. With increasing the spacer length, the POSS core and the Tp arms gradually decoupled. For example, when the spacer length increased to C₆, a lamellar morphology with a rectangular columnar symmetry was observed by TEM. Finally, when the spacer length increased to C₁₀, an inverted columnar morphology with four Tp columns forming a super column in the POSS/alkyl chain matrix was observed by TEM, and an oblique columnar symmetry was determined for the molecular packing by XRD. Such self-

assemblies are a result of the well-known interplay of microphase segregation and the competition between interactions among peripheral mesogens and the decreased entropy due to the deformation of the core.

Acknowledgment. This work was supported by NSF CAREER Award DMR-0348724, DuPont Young Professor Grant, and 3M Nontenured Faculty Award. The synchrotron X-ray experiments were carried out at the National Synchrotron Light Source, Brookhaven National Laboratory, supported by the U.S. Department of Energy. Assistance from Dr. Lixia Rong and Prof. Benjamin Hsiao at State University of New York at Stony Brook for synchrotron X-ray experiments is highly acknowledged.

Supporting Information Available: Observed and calculated spacings for different reflections in POSS(12Tp)₈ samples **4–6**; Temperature-dependent FTIR spectra for samples **4–6**. This material is available free of charge via the Internet at <http://pubs.acs.org>.

References and Notes

- Saez, I. M.; Goodby, J. W. *J. Mater. Chem.* **2005**, *15*, 26–40.
- Kato, T.; Mizoshita, N.; Kishimoto, K. *Angew. Chem., Int. Ed.* **2006**, *45*, 38–68.
- Percec, V.; Glodde, M.; Bera, T. K.; Miura, Y.; Shiyanovskaya, I.; Singer, K. D.; Balagurusamy, V. S. K.; Heiney, P. A.; Schnell, I.; Rapp, A.; Spiess, H. W.; Hudson, S. D.; Duan, H. *Nature* **2002**, *419*, 384–387.
- Percec, V.; Dulcey, A. E.; Balagurusamy, V. S. K.; Miura, Y.; Smidral, J.; Peterca, M.; Nummelin, S.; Edlund, U.; Hudson, S. D.; Heiney, P. A.; Duan, H.; Magonov, S. N.; Vinogradov, S. A. *Nature* **2004**, *430*, 764–768.
- Percec, V.; Dulcey, A. E.; Peterca, M.; Ilies, M.; Sienkowska, M. J.; Heiney, P. A. *J. Am. Chem. Soc.* **2005**, *127*, 17902–17909.
- Percec, V.; Glodde, M.; Peterca, M.; Rapp, A.; Schnell, I.; Spiess, H. W.; Bera, T. K.; Miura, Y.; Balagurusamy, V. S. K.; Aqad, E.; Heiney, P. A. *Chem.—Eur. J.* **2006**, *12*, 6298–6314.
- Percec, V.; Dulcey, A. E.; Peterca, M.; Ilies, M.; Nummelin, S.; Sienkowska, M. J.; Heiney, P. A. *Proc. Natl. Acad. Sci. U.S.A.* **2006**, *103*, 2518–2523.
- Percec, V.; Dulcey, A. E.; Peterca, M.; Ilies, M.; Nummelin, S.; Sienkowska, M. J.; Heiney, P. A. *J. Am. Chem. Soc.* **2006**, *128*, 6713–6720.
- Donnio, B.; Buathong, S.; Bury, I.; Guillou, D. *Chem. Soc. Rev.* **2007**, *36*, 1495–1513.
- Tschierske, C. *J. Mater. Chem.* **2001**, *11*, 2647–2671.
- McKenna, M. D.; Barbera, J.; Marcos, M.; Serrano, J. L. *J. Am. Chem. Soc.* **2005**, *127*, 619–625.
- Percec, V.; Chu, P. W.; Kawasumi, M. *Macromolecules* **1994**, *27*, 4441–4453.
- Percec, V.; Chu, P. W.; Ungar, G.; Zhou, J. *J. Am. Chem. Soc.* **1995**, *117*, 11441–11454.
- Percec, V. *Pure Appl. Chem.* **1995**, *67*, 2031–2038.
- Lorenz, K.; Holter, D.; Stuhn, B.; Mulhaupt, R.; Frey, H. *Adv. Mater.* **1996**, *8*, 414–426.
- Ponomarenko, S. A.; Rebrov, E. A.; Bobrovsky, A. Y.; Boiko, N. I.; Muzaferov, A. M.; Shibaev, V. P. *Liq. Cryst.* **1996**, *21*, 1–12.
- Baars, M.; Sontjens, S. H. M.; Fischer, H. M.; Peerlings, H. W. I.; Meijer, E. W. *Chem.—Eur. J.* **1998**, *4*, 2456–2466.
- Barbera, J.; Gimenez, R.; Marcos, M.; Serrano, J. L. *Liq. Cryst.* **2002**, *29*, 309–314.
- Barbera, J.; Marcos, M.; Serrano, J. L. *Chem.—Eur. J.* **1999**, *5*, 1834–1840.
- Serrano, J. L.; Marcos, M.; Martin, R.; Gonzalez, M.; Barbera, J. *Chem. Mater.* **2003**, *15*, 3866–3872.
- Marcos, M.; Gimenez, R.; Serrano, J. L.; Donnio, B.; Heinrich, B.; Guillou, D. *Chem.—Eur. J.* **2001**, *7*, 1006–1013.
- Donnio, B.; Barbera, J.; Gimenez, R.; Guillou, D.; Marcos, M.; Serrano, J. L. *Macromolecules* **2002**, *35*, 370–381.
- Ponomarenko, S. A.; Boiko, N. I.; Shibaev, V. P.; Richardson, R. M.; Whitehouse, I. J.; Rebrov, E. A.; Muzaferov, A. M. *Macromolecules* **2000**, *33*, 5549–5558.
- Rueff, J. M.; Barbera, J.; Donnio, B.; Guillou, D.; Marcos, M.; Serrano, J. L. *Macromolecules* **2003**, *36*, 8368–8375.
- Rueff, J. M.; Barbera, J.; Marcos, M.; Omenat, A.; Martin-Rapun, R.; Donnio, B.; Guillou, D.; Serrano, J. L. *Chem. Mater.* **2006**, *18*, 249–254.
- Busson, P.; Ortegren, J.; Ihre, H.; Gedde, U. W.; Hult, A.; Andersson, G. *Macromolecules* **2001**, *34*, 1221–1229.

- (27) Cameron, J. H.; Facher, A.; Lattermann, G.; Diele, S. *Adv. Mater.* **1997**, *9*, 398–403.
- (28) Maliszewskyj, N. C.; Heiney, P. A.; Josefowicz, J. Y.; Plesnivy, T.; Ringsdorf, H.; Schuhmacher, P. *Langmuir* **1995**, *11*, 1666–1674.
- (29) Grafe, A.; Janietz, D.; Frese, T.; Wendorff, J. H. *Chem. Mater.* **2005**, *17*, 4979–4984.
- (30) Paraschiv, I.; Giesbers, M.; van Lagen, B.; Grozema, F. C.; Abellon, R. D.; Siebbeles, L. D. A.; Marcelis, A. T. M.; Zuilhof, H.; Sudholter, E. J. R. *Chem. Mater.* **2006**, *18*, 968–974.
- (31) Paraschiv, I.; de Lange, K.; Giesbers, M.; van Lagen, B.; Grozema, F. C.; Abellon, R. D.; Siebbeles, L. D. A.; Sudholter, E. J. R.; Zuilhof, H.; Marcelis, A. T. M. *J. Mater. Chem.* **2008**, *18*, 5475–5481.
- (32) Bisoyi, H. K.; Kumar, S. *Tetrahedron Lett.* **2008**, *49*, 3628–3631.
- (33) Gupta, S. K.; Raghunathan, V. A.; Kumar, S. *New J. Chem.* **2009**, *33*, 112–118.
- (34) Plesnivy, T.; Ringsdorf, H.; Schuhmacher, P.; Nuetz, U.; Diele, S. *Liq. Cryst.* **1995**, *18*, 185–90.
- (35) Zelcer, A.; Donnio, B.; Bourgogne, C.; Cukiernik, F. D.; Guillon, D. *Chem. Mater.* **2007**, *19*, 1992–2006.
- (36) Jeong, K. U.; Jing, A. J.; Mansdorf, B.; Graham, M. J.; Yang, D. K.; Harris, F. W.; Cheng, S. Z. D. *Chem. Mater.* **2007**, *19*, 2921–2923.
- (37) Imrie, C. T.; Lu, Z.; Picken, S. J.; Yildirim, Z. *Chem. Commun.* **2007**, 1245–1247.
- (38) Zhi, L.; Wu, J.; Mullen, K. *Org. Lett.* **2005**, *7*, 5761–5764.
- (39) Levelut, A. M.; Moriya, K. *Liq. Cryst.* **1996**, *20*, 119–124.
- (40) Moriya, K.; Suzuki, T.; Yano, S.; Miyajima, S. *J. Phys. Chem. B* **2001**, *105*, 7920–7927.
- (41) Xu, J. W.; Ling, T. C.; He, C. B. *J. Polym. Sci., Part A: Polym. Chem.* **2008**, *46*, 4691–4703.
- (42) Barbera, J.; Bardaji, M.; Jimenez, J.; Laguna, A.; Martinez, M. P.; Oriol, L.; Serrano, J. L.; Zaragozano, I. *J. Am. Chem. Soc.* **2005**, *127*, 8994–9002.
- (43) Barbera, J.; Jimenez, J.; Laguna, A.; Oriol, L.; Perez, S.; Serrano, J. L. *Chem. Mater.* **2006**, *18*, 5437–5445.
- (44) Chuard, T.; Deschenaux, R. *Helv. Chim. Acta* **1996**, *79*, 736–741.
- (45) Dardel, B.; Deschenaux, R.; Even, M.; Serrano, E. *Macromolecules* **1999**, *32*, 5193–5198.
- (46) Chuard, T.; Deschenaux, R.; Hirsch, A.; Schonberger, H. *Chem. Commun.* **1999**, 2103–2104.
- (47) Dardel, B.; Guillon, D.; Heinrich, B.; Deschenaux, R. *J. Mater. Chem.* **2001**, *11*, 2814–2831.
- (48) Felder-Flesch, D.; Rupnicki, L.; Bourgogne, C.; Donnio, B.; Guillon, D. *J. Mater. Chem.* **2006**, *16*, 304–309.
- (49) Lenoble, J.; Maringa, N.; Campidelli, S.; Donnio, B.; Guillon, D.; Deschenaux, R. *Org. Lett.* **2006**, *8*, 1851–1854.
- (50) Maringa, N.; Lenoble, J.; Donnio, B.; Guillon, D.; Deschenaux, R. *J. Mater. Chem.* **2008**, *18*, 1524–1534.
- (51) Mehl, G. H.; Goodby, J. W. *Angew. Chem., Int. Ed.* **1996**, *35*, 2641–2643.
- (52) Goodby, J. W.; Mehl, G. H.; Saez, I. M.; Tuffin, R. P.; Mackenzie, G.; Auzely-Velty, R.; Benvegnu, T.; Plusquellec, D. *Chem. Commun.* **1998**, 2057–2070.
- (53) Saez, I. M.; Goodby, J. W. *Liq. Cryst.* **1999**, *26*, 1101–1105.
- (54) Mehl, G. H.; Saez, I. M. *Appl. Organomet. Chem.* **1999**, *13*, 261–272.
- (55) Kreuzer, F. H.; Maurer, R.; Spes, P. *Makromol. Chem., Macromol. Symp.* **1991**, *50*, 215–228.
- (56) Elsasser, R.; Mehl, G. H.; Goodby, J. W.; Photinos, D. *J. Chem. Commun.* **2000**, 851–852.
- (57) Saez, I. M.; Goodby, J. W. *J. Mater. Chem.* **2001**, *11*, 2845–2851.
- (58) Saez, I. M.; Goodby, J. W.; Richardson, R. M. *Chem.—Eur. J.* **2001**, *7*, 2758–2764.
- (59) Laine, R. M.; Zhang, C.; Sellinger, A.; Viculis, L. *Appl. Organomet. Chem.* **1998**, *12*, 715–723.
- (60) Zhang, C.; Bunning, T. J.; Laine, R. M. *Chem. Mater.* **2001**, *13*, 3653–3662.
- (61) Karahaliou, P. K.; Kouwer, P. H. J.; Meyer, T.; Mehl, G. H.; Photinos, D. *J. Soft Matter* **2007**, *3*, 857–865.
- (62) Karahaliou, P. K.; Kouwer, P. H. J.; Meyer, T.; Mehl, G. H.; Photinos, D. *J. Phys. Chem. B* **2008**, *112*, 6550–6556.
- (63) Pan, Q.; Chen, X.; Fan, X.; Shen, Z.; Zhou, Q. *J. Mater. Chem.* **2008**, *18*, 3481–3488.
- (64) Cui, L.; Collet, J. P.; Xu, G.; Zhu, L. *Chem. Mater.* **2006**, *18*, 3503–3512.
- (65) Sun, L.; Liu, Y. X.; Zhu, L.; Hsiao, B. S.; Avila-Orta, C. A. *Polymer* **2004**, *45*, 8181–8193.
- (66) Miao, J.; Zhu, L. *Chem. Mater.* **2010**, *22*, 197–206.
- (67) Wang, T.; Yan, D.; Luo, J.; Zhou, E.; Karthaus, O.; Ringsdorf, H. *Liq. Cryst.* **1997**, *23*, 869–878.
- (68) Miao, J.; Cui, L.; Lau, H. P.; Mather, P. T.; Zhu, L. *Macromolecules* **2007**, *40*, 5460–5470.
- (69) Wu, P.; Zeng, Q.; Xu, S.; Wang, C.; Yin, S.; Bai, C. L. *ChemPhysChem* **2001**, *2*, 750–754.

JP910053E